The agricultural expansion in South America's Dry Chaco: Regional hydroclimate effects

M. Agostina Bracalenti[1,2], Omar V. Müller[1,2], Miguel A. Lovino[1,2], E. Hugo Berbery[3]

[1]Consejo Nacional de Investigaciones Científicas y Técnicas (CONICET), Santa Fe, Argentina.

5 [2]Centro de Variabilidad y Cambio Climático (CEVARCAM), Facultad de Ingeniería y Ciencias Hídricas (FICH), Universidad Nacional del Litoral (UNL), Santa Fe, Argentina.

[3]Earth System Science Interdisciplinary Center (ESSIC)/Cooperative Institute for Satellite Earth System Studies (CISESS), University of Maryland, College Park, MD, USA

Correspondence to: Omar V. Müller (ovmuller@unl.edu.ar)

10 **Abstract.** The Gran Chaco ecoregion is South America's largest remaining continuous stretch of dry forest. It has experienced intensive deforestation, mainly in the western part known as Dry Chaco, resulting in the highest rate of dry forest loss globally between 2000 and 2012. The replacement of natural vegetation with other land uses modifies the surface's biophysical properties, affecting heat and water fluxes and modifying the regional climate. This study examines land use and land cover changes (LULCCs) in Dry Chaco from 2001 to 2015, their effects on local and non-local climate, 15 and explores the potential impacts of future agricultural expansion in the region. To this end, Weather Research and Forecasting (WRF) model simulations are performed for two scenarios: the first one evaluates the observed land cover changes between 2001 and 2015 that covered 8% of the total area of Dry Chaco; the second scenario assumes an intensive agricultural expansion within the Dry Chaco. In both scenarios, deforestation processes lead to decreases in LAI, increases in albedo, and reductions in stomatal resistance, reducing the net surface radiation and, correspondingly, a decrease in turbulent 20 fluxes suggesting a decline in available energy in the boundary layer. The result is an overall weakening of the water cycle in the Dry Chaco and, most prominently, implies a reduction in precipitation. A feedback loop develops since dry soil absorbs significantly less solar radiation than moist soil. Finally, the simulations suggest that the Dry Chaco would intensify its aridity, extending the drier and hotter conditions into the Humid Chaco.

1 Introduction

25 The expansion of the agricultural frontier in southern South American countries (Brazil, Paraguay, Argentina, and Uruguay) has been favoured by natural, technological, economic, and socio-cultural factors. Large areas of South America have experienced a significant increase in land use and land-cover changes (LULCCs), mostly of anthropogenic origin (Gasparri and Grau, 2009). The regional increase in annual average rainfall in arid regions, combined with biotechnological advances, strengthened the crops' adaptability to adverse climate conditions and enhanced the availability of productive lands. 30 Moreover, the availability of cheap land and labour, the lack of environmental regulations or their inadequate enforcement,

and the increased food demand from new international markets in the last decades contributed to the agricultural expansion advancing on native vegetation (Dros, 2004; Paruelo et al., 2005).

The Gran Chaco ecoregion combines all the previous factors, leading to an intensive deforestation process, mainly in the
35   western part known as Dry Chaco (Boletta et al., 2006; Zak et al., 2008). The eastern part is known as Humid Chaco. The Gran Chaco is the largest remaining continuous stretch of dry forest in South America (Gasparri and Grau, 2009; Portillo-Quintero and Sanchez-Azofeifa, 2010; Fehlenberg et al., 2017). Only 9 % of it is currently protected (Nori, 2016), and consequently, it is one of the most threatened ecoregions worldwide (Kummerle, 2017). Due to agricultural expansion, the Gran Chaco is one of the largest global deforestation hotspots, reaching the highest rate of dry forest loss worldwide (Hansen
40   et al., 2013; Volante et al. 2016). The Gran Chaco underwent deforestation of 78,000 km^2 between 2001 and 2012, with varying deforestation rates, from ~2,900 km^2 year^{-1} during 2001-2002 to ~9,200 km^2 year^{-1} during 2007-2008 (Fehlenberg et al., 2017). In particular, dry forest deforestation rates in the Argentinian part of Gran Chaco during the 2000s became up to three times higher than in the 1980s (Piquer-Rodríguez et al., 2015).

45   LULCCs affect the soil state and the overlying atmosphere through the influence of the soil conditions on the land-atmosphere interactions (Dirmeyer et al., 2000). This is particularly evident in southern South America, where the land-atmosphere coupling shows strong relationships between the water cycle components (Spennemann and Saulo, 2015; Ruscica et al., 2016; Martínez et al., 2016; Müller et al., 2021a). The replacement of natural vegetation by pastures, crops, or other types of land use modifies biophysical properties related to vegetation (albedo, stomatal resistance, surface roughness,
50   among others), altering the ecosystem functioning and the surface fluxes (Lee and Berbery, 2012; Müller et al., 2014; Baldi et al., 2015). For instance, when crops replace forests, groundwater uptake and transpiration are reduced due to the lack of deep roots in crops. This mechanism induces the rise of the water table level, facilitating soil saturation, increasing surface runoff and, therefore, the probability of occurrence of floods or waterlogging (Miguez-Macho et al., 2007a; Jobbagy et al., 2008; Martínez et al., 2016).

55

A meta-analysis performed by Sirimarco et al. (2018) based on more than 100 scientific papers about land cover changes in different parts of the world found that replacing grasslands with forests (afforestation) may increase infiltration and evapotranspiration by up to 65 % and 30 %, respectively. Still, when crops replace pastures, water infiltration is significantly reduced without major changes in evapotranspiration. In brief, the changes in soil conditions affect the energy and water
60   fluxes on the surface, which in turn modify the atmospheric fluxes (e.g., moisture transport) (Lee and Berbery, 2012; Mahmood et al., 2014). Thus, LULCCs inevitably alter the local climate state, but they may also impact adjacent or remote areas due to changes in river flow or atmospheric dynamics (Mahmood et al., 2010).

This study addresses the following questions: How do LULCCs in the Dry Chaco alter the land surface processes locally? And, what are the local and non-local effects of LULCCs on the Gran Chaco? A suitable way to comprehensively tackle these questions is using regional climate model (RCM) simulations. RCMs have two components -the land surface and the atmosphere- that interact at each time step through surface fluxes, enabling feedback between the atmosphere and the soil. This feature is key to uncovering the atmospheric response to LULCCs. Land cover types and their associated biophysical properties are usually prescribed in Land Surface Models (LSMs), the land component of RCMs. Then, sensitivity experiments can be conducted by updating the land cover map or artificially modifying the land cover to simulate potential scenarios of LULCCs.

To address the questions raised above, we adopt a comprehensive three-step methodology. First, we evaluate the dominant LULCC in Dry Chaco during the current century using state-of-the-art satellite information (the Moderate Resolution Imaging Spectroradiometer, MODIS). Second, we analyse the local effects of current LULCCs in Dry Chaco by assessing simulations performed for the same period but using MODIS land cover maps of different years with the Weather Research and Forecasting (WRF) model. Third, we investigate the remote effects of LULCCs in Humid Chaco by analysing WRF simulations that assume a progressive expansion of the agricultural frontier in Dry Chaco. Section 2 describes the region of interest, the observational data, and the experiments and evaluates the performance of the WRF control simulations. Section 3 presents the analysis of the model simulation responses to different LULC scenarios. Finally, the discussion and concluding remarks are presented in Section 4.

2 Data, model, and experiments

2.1 Study Region

2.1.1 Geographical features

The Gran Chaco is a natural region of about 1,100,000 km^2 stretching from northern Argentina to southeastern Bolivia and northwestern Paraguay (Fig. 1). In South America, it is the second-largest forest after the Amazon and the largest remaining continuous stretch of dry forest (Bucher and Huszar, 1999; Portillo-Quintero and Sánchez-Azofeifa, 2010). The Gran Chaco is characterised by a flat topography with elevations varying between 100 and 500 m. The region is part of the subtropical belt, with a latitudinal south-north thermal gradient with a mean annual temperature ranging from 19 °C to 24 °C (Bucher, 1982). The region shows a pronounced longitudinal gradient in precipitation, dividing the Gran Chaco into two distinct subregions: the Dry Chaco and the Humid Chaco (as indicated by the borders in Fig. 1). The Dry Chaco is dominated by a semi-arid climate with annual precipitation ranging from 450 to 900 mm. The Humid Chaco presents a humid subtropical climate with annual precipitation of about 900–1200 mm (Bucher, 1982).

95 The Gran Chaco is one of the most dramatic global deforestation hotspots, with the highest rate of dry forest loss in the world in the 2000-2012 period (Hansen et al., 2013), due to the expansion of soybean production and cattle ranching (Fehlenberg et al., 2017). The Humid Chaco has been intensively transformed into agriculture, while the Dry Chaco remained largely forested because agriculture methods depended on rain, making it unprofitable despite high soil fertility and flat terrain (Bucher and Huszar, 1999). This historical behaviour has changed in recent decades due to the westward shift

100 of the isohyets in the Gran Chaco and the availability of climate-resistant seeds (Dros et al., 2004; Boletta et al., 2006; Zak et al., 2008).

2.1.2 Land cover and its evolution in Dry Chaco

The dominant land cover in the Dry Chaco and its evolution from 2001 to 2015 are evaluated using land use maps derived from the MODIS Land Cover Climate Modeling Grid Product MCD12C1. The product is provided as a global mosaic at

105 0.05° grid spacing and follows the International Geosphere–Biosphere Program (IGBP) classification.

The top land cover categories in the region, as observed in 2015, are savanna, woody savanna, forest, grassland, shrubland, and cropland (Fig. 2a). Figure 2b shows how the dominant land cover categories in Dry Chaco evolved from 2001 to 2015. For simplicity, some of the IGBP types were grouped into major land cover classes on this panel. For instance, forest

110 includes evergreen broadleaf, deciduous broadleaf, and mixed forests; shrubland includes closed and open shrublands, while cropland includes cropland and cropland/natural vegetation mosaic. The land cover evolution indicates that agricultural lands (cropland and grassland) increased mainly up to 2007. Between 2001 and 2015, agriculture coverage increased by 15.4 %, representing 2.6 % of the total area of the Dry Chaco. On the other hand, forests and woody savanna decreased by 1.5 % and 16.4 %, respectively, representing 4.3 % of the Dry Chaco area.

115

Figure 2c indicates that 18 % of the Dry Chaco area suffered LULCCs from 2001 to 2015. These changes are quantified per category in Fig. 2d. Most of these changes (52 %) involve transitioning from categories characterised by higher tree coverage to others with lower coverage, which could be associated with deforestation processes. According to Fig. 2d, they are:

120
- from woody savanna to savanna, 23,328 km^2,
- from savanna to agriculture, 12,672 km^2 (40 % to cropland and 60 % to grassland),
- from woody savanna to agriculture, 10,368 km^2 (50 % to cropland and 50 % to grassland)
- from forest to savanna, 8,064 km^2,
- from forest to woody savanna, 6,336 km^2,
125
- from forest to agriculture, 6,192 km^2 (67 % to cropland and 33 % to grassland), and
- from open shrubland to grassland, 5,904 km^2.

Note that about 31 % of the area corresponds to changes called "others" that consist in changes that are not linked to deforestation processes (e.g., from open shrubland to savanna or to barren, from grassland to cropland, among others). Curiously, about 17 % of the changes are from savanna and woody savanna to deciduous broadleaf forests. This
130 transformation between natural land covers in a short period (14 years) is unthinkable in the real world and may be an artefact of the computation algorithms (Liang and Gong, 2010; Cai et al., 2014). These changes are named as illogical in Fig. 1c.

2.2 The WRF model and its configuration

The numerical simulations were performed with the WRF model in its Advanced Research WRF (ARW) version 3.9. The
135 WRF was run with a horizontal grid spacing of 12 km and 38 vertical levels over a domain that covers the southern part of South America, which includes the Gran Chaco (see Fig. 1). The model physics configuration is summarised in Table 1. The parameterisations follow the selection of schemes and options tested by Lee and Berbery (2012), who reported they minimise biases in simulations for South America. Moreover, this configuration demonstrated high performance in long-term simulations (Müller et al. 2014) and short-term weather forecasts (Müller et al. 2016) in southern South America. The
140 model was forced by the initial and 6-hr boundary conditions obtained from the National Centers for Environmental Prediction (NCEP) Climate Forecast System Version 2 (CFSv2, Saha et al., 2014).

The WRF atmospheric component is coupled with the Noah-MP LSM (Niu et al., 2011), which solves the surface energy and water balances linking the surface conditions with the atmosphere. Noah-MP is an improved version of the Noah LSM
145 (Chen et al. 1996; Chen and Dudhia, 2001), including multiple parameterisation options for selected physical processes. It has four soil layers with a corresponding thickness of 10, 30, 60, and 100 cm from top to bottom (2 m total depth). Further characteristics are listed in Table 2.

2.3 Experimental design

Sensitivity experiments were performed to determine how LULCC in Dry Chaco may influence the regional hydroclimate.
150 Three sets of simulations (ensembles) were conducted for the same period (January 2014 to June 2016), using different land cover maps (see Fig. 3). Each ensemble has four members with identical parameterisations, with the only difference being the initial conditions that are 24-hr apart, following the lagged average forecasting method (Hoffman and Kalnay, 1983).

The CONTROL ensemble employs the MODIS land cover map corresponding to 2015 (Fig. 2a). The PAST ensemble uses
155 the MODIS land cover map for the year 2001 (Fig. 4a). The FUTURE ensemble assumes an intensive agricultural expansion within Dry Chaco (Fig. 4b), mimicking what could be expected in the future if current expansion trends are to continue. The corresponding land cover map is a modified version of the 2015 land cover map in which a dilation method (Gonzalez and Woods, 1993) is applied over agricultural grid cells within the Dry Chaco. This method expands all crop/grassland areas by

adding surrounding grid cells to the boundaries of the agriculture areas. In the resulting land cover map, croplands cover

160   29.4% while grasslands cover 19.1% of the Dry Chaco area, meaning that the areas occupied by crops and pastures have

been expanded by 5 and 2.5 times, respectively.

The differences between the CONTROL and the PAST ensembles will be called the 'observed LULCCs' scenario

(OBS_LULCC). This scenario is employed to assess the impact of the land cover changes that occurred since 2001 on the

165   2014-2016 climate of the Dry Chaco. The differences between the FUTURE and the CONTROL ensembles are referred to

as a scenario of 'agricultural intensification' (AG_INT). This scenario is used to evaluate the response of the 2014-2016

climate had there been a preceding large agricultural expansion in Dry Chaco. It is well known that land cover changes have

been extensive over the south of South America outside the Gran Chaco, so other effects may come into play affecting the

climate of Humid Chaco (Salazar et al., 2015), however these other factors are not part of the current study.

170   **2.4 Model evaluation**

2.4.1 Evaluation datasets

The performance of the CONTROL ensemble is evaluated by comparing simulated precipitation, soil moisture, and 2m

temperature against observational data sets, either from satellite sources or gridded observations. Three different

precipitation datasets are employed. First, the NCEP's Climate Prediction Center (CPC) Unified Gauge-Based Analysis of

175   Global Daily Precipitation (Chen et al., 2008; Xie et al., 2010). This dataset consists of daily rain gauge observations

interpolated to a $0.5° \times 0.5°$ grid. The second dataset, also at $0.5°$ grid spacing, is the Climate Research Unit (CRU) monthly

precipitation dataset. The CRU TS v. 4.03 dataset is based on analysing more than 4000 meteorological stations (Harris et

al., 2020). Lastly, we use the three hourly precipitation in the WATCH Forcing Data methodology applied to ERA-Interim

reanalysis data (WFDEI) (Weedon et al., 2014). Note that the three datasets overlap in their sources.

180

Soil moisture is assessed at two model layers: 0-10 cm and 0-100 cm. The top layer (10 cm) is compared against the Soil

Moisture Operational Products System (SMOPS; Liu et al., 2016). This product combines soil moisture retrievals from

multiple satellite sensors producing global soil moisture maps as a volumetric content near the surface (top 1-5 cm) at daily

intervals and at a $0.25°$ grid spacing (Liu et al., 2016). Observed and simulated near-surface soil moisture are compared in

185   terms of volumetric water content ($m^3 m^{-3}$) to minimise the impact of the thickness differences. The root zone soil moisture

(100 cm), crucial for vegetation growth, is evaluated with the operational product H14-SM-DAS-2 developed at the

EUMETSAT Satellite Application Facility on Support to Operational Hydrology and Water Management (HSAF). This

product gives estimates of root zone soil moisture at daily intervals on a 25 km $\times$ 25 km grid (Albergel et al., 2012).

190 Temperature is evaluated with two products: the CRU TS v. 4.03 global monthly surface air temperature data set and the WFDEI three hourly temperature. Both are provided at a grid spacing of 0.5°.

2.4.2 Precipitation

The spatial pattern of the observation-based precipitation for the simulation period presents maximum values in southern Brazil, eastern Paraguay, and northeastern Argentina (Figure 5a), where the precipitation rate is ~5 mm day^{-1}. This
195 magnitude gradually decreases westward to less than ~1 mm day^{-1} on top of the Andes Mountains and the desert of Atacama. The mean WRF precipitation field (Fig. 5b) reveals a similar spatial structure to the observations but with weaker values in the wet part, where the model simulates drier rainfall (see Fig. 5c). On the other hand, WRF simulates wetter conditions over the Altiplano (high plateau in Bolivia). Wet anomalies over mountainous regions are often attributed to model limitations and uncertainties in gridded observations and satellite estimates (Adam et al., 2006; Beck et al., 2017; Müller et al., 2021b).
200

Focusing on the Gran Chaco, the model simulations show almost no biases in the Dry Chaco and present dry biases of ~1-2 mm day^{-1} in the Humid Chaco. The drier conditions arise from underestimated late summer and autumn rain, as shown in Figure 5d. Conversely, WRF notably improves the estimation in winter (the dry season) and spring, showing almost the same peaks as observations for all years. The correlation and the error estimates confirm the good performance of WRF in
205 the Gran Chaco. The monthly temporal correlation between the area-averaged observed and simulated precipitation is r=0.93 for the Dry Chaco and r=0.85 for the Humid Chaco. The RMSEs are 0.6 mm day^{-1} and 1.9 mm day^{-1}, respectively.

2.4.3 Soil Moisture

The SMOPS satellite estimate of near-surface soil moisture exhibits high values to the east and a decreasing gradient toward the west (Fig. 6a), following the precipitation pattern. The simulated soil moisture content shows a remarkable spatial
210 structure and magnitude agreement in most of the domain, except over the Altiplano where the wet precipitation biases produce wet soils (Fig. 6b). The resemblance is even more evident over the Gran Chaco (Fig. 6c). In terms of temporal evolution, the area-averaged simulated soil moisture presents similarities with SMOPS (r=0.61 for Humid Chaco and r=0.55 for Dry Chaco) but with a slight systematic overestimation (Fig. 6g).

215 The simulated root-zone soil moisture also presents a notable overall resemblance to the HSAF satellite estimates (Fig. 6d-e), with slight dry biases towards east, likely derived from the dry precipitation biases shown for the same area (see Fig. 5c). Focusing on the Gran Chaco, the area-averaged WRF soil moisture presents a similar evolution to HSAF, but with a systematic negative bias (Fig. 6g), that can also be attributed to precipitation biases (Fig. 5d). It is important to highlight that the performance is clearly different for the sub-regions. The Dry Chaco presents a strong spatial agreement with HSAF
220 (RMSE=0.035), but weak temporal correlation (r=0.33), while the Humid Chaco presents a high temporal correlation (r=0.88) but higher dry biases in space (RMSE=0.091).

2.4.4 Temperature

The spatial distribution of the time-mean observed temperature shows a latitudinal gradient with maximum values over the central-northern domain decreasing toward the south (Fig. 7a). The warmer region has an average temperature above 25 °C
225   that gradually decreases southward to less than 15 °C. The coldest region over the high-altitude Andes Mountains has average temperatures below 5 °C.

Figure 7b shows that the simulated temperature's spatial pattern captures the observation-based products' main features in terms of distribution and magnitude (Fig. 7c), especially in flat areas (see Fig. 1). In high-altitude regions, the model
230   produces cold biases. For the Gran Chaco, WRF shows slight warm and cool biases (about ±1 °C) in parts of Dry Chaco and Humid Chaco, respectively. The simulated temperature evolution in the Gran Chaco is remarkably similar to observations (r=0.97 for Humid Chaco and r=0.98 for Dry Chaco), with slightly higher seasonal variability (Fig. 7d).

3 Experiments' results

This section examines the two scenarios (OBS_LULCC and AG_INT) presented in Section 2.3. In both cases, simulations
235   were carried out for 2014-2016 just changing the corresponding land cover maps. In both scenarios, the analysis is conducted during the austral summer months (DJF), when vegetation is highly active, and land-atmosphere interactions are intensified in the Gran Chaco ecoregion (Müller et al., 2021a). Throughout the analysis, we will refer to local effects as those that pertain to the grid points within Dry Chaco that experienced LULCCs (purple grid cells in Fig. 4c-d). Non-local effects are those found at grid points that did not undergo any land cover change in the remaining Dry Chaco area (blank areas in Fig.
240   4c). Lastly, remote effects encompass those observed in the Humid Chaco area (blank areas within the blue limits in Fig. 4d).

3.1 Scenario OBS_LULCC: Actual LULC changes from 2001 to 2015

Almost 20 % of the Dry Chaco's land cover changed from 2001 to 2015 (see Section 2.1.2). Figures 8a-c show the changes in biophysical properties that are particularly sensitive to the observed LULCCs: leaf area index (LAI), albedo, and stomatal resistance. The changes in properties are spread over the small fragmented areas that underwent LULCCs. The decrease in
245   LAI, increase in albedo, and reduction in stomatal resistance in the Dry Chaco's centre-east, northeast, and west boundaries are associated with deforestation processes (orange grid cells in Fig. 2c). On the other hand, other areas showing increases in LAI and stomatal resistance, and decreases in albedo are not associated with deforestation as discussed in Section 2.1.2.

3.1.1 Effects on the energy budget

The changes in biophysical properties lead to the uneven distribution of positive and negative changes in the radiation fluxes
250   (Figs. 9a-c). The net radiation pattern is primarily influenced by variations in shortwave radiation, while changes in longwave radiation are minimal due to negligible emissivity variations. On average, the areas that underwent local LULCCs

experienced a ~2 % reduction in net radiation, which aligns with the overall increase in albedo (Fig. 8b) and the consequent enhancement of outgoing shortwave radiation. In the remaining areas of Dry Chaco, where land cover was not changed, positive and negative changes up to ±10 W m^{-2} balance each other, resulting in a near-zero areal average.

255

The changes in net radiation alter the main components of the energy balance, i.e., the sensible heat flux and the latent heat flux. The spatial distributions of sensible and latent heat fluxes play important roles in determining near-surface temperature. Figures 9d-e reveal a similar spatial pattern but with opposite signs for changes in sensible heat and latent heat. As with the radiation terms, the changes are of the order of ±10 W m^{-2}. Furthermore, Fig. 9f shows that the deforested areas in the

260 northern and central eastern zones of Dry Chaco experience warming, while the southern area exhibits cooling. Both of these changes can be attributed to variations in sensible heat flux. On average, the changes in net radiation lead to an average decrease of -3.5 % in sensible heat at the local level and 0.6 % in the remaining Dry Chaco (Fig. 9e). Latent heat exhibits minor or negligible changes over the whole Dry Chaco (Fig. 9d). Despite the presence of locally strong signals (up to ±0,4 °C), the spatially averaged temperature changes present a slight rise due to the compensatory warming and cooling effects.

265 **3.1.2 Effects on the water cycle**

The changes in biophysical properties lead to overall drier conditions in Dry Chaco, with precipitation decreasing by about -1.7 % on average. However, there is a significant spatial heterogeneity with precipitation changes ranging from -29 mm month^{-1} to +35 mm month^{-1}, even in areas that conserved the land cover (Fig. 10a). Soil moisture (Fig. 10b) follows the spatial pattern of precipitation, with net negative changes in both local (-2.6 %) and non-local (-0.7 %) areas.

270 Evapotranspiration also follows the patterns of precipitation and soil moisture, although the net changes are negligible (see inset in Fig 10c). Note that stomatal resistance is strongly reduced in deforested areas, which would facilitate plant transpiration and consequently higher evapotranspiration. Our interpretation is that plants cannot take advantage of the open stomata due to the dry soils, given that Dry Chaco is a region where soil moisture availability limits the evapotranspiration regime. The reduced precipitation and drier soils end up affecting the total runoff, which presents a net reduction in the Dry

275 Chaco of -2.1 % in local areas and -5.5 % in non-local areas (Fig. 10d). These results suggest that the observed LULCCs in just 14 years can weaken the water cycle in Dry Chaco, leading this arid region to even drier summers, eventually increasing its exposure and vulnerability to extremes.

3.2 Scenario AG_INT: Intensive expansion of the agricultural land

The changes in surface properties in the OBS_LULCC scenario have a granular structure that illustrates the realistic ways

280 deforestation progresses. Unlike the OBS_LULCC scenario, the AG_INT scenario shows changes in LAI, albedo, and stomatal resistance that exhibit spatial continuity, consistent with the assumed idealised LULCCs. In this AG_INT scenario, the expansion of crops and grasslands covers 64 % of the Dry Chaco. Figs. 11a-c illustrate that replacing native vegetation with grasslands and croplands leads to a general reduction in LAI and stomatal resistance, as well as an increase in albedo.

Interestingly, the anthropisation of certain native covers results in "greener" conditions, in line with the prescribed values of
285 the biophysical properties applied by the LSM. For instance, Noah-MP prescribes a higher LAI for grassland (1.7) than open
shrubland (1.6).

3.2.1 Effects on the energy budget

The intensive expansion of agriculture simulated in Dry Chaco resulted in an overall decrease in net total radiation, which is
reduced by -9.5 % (Fig. 12c). This reduction is primarily due to changes in shortwave radiation (Fig. 12a). Areas where
290 LULCCs are imposed present higher albedo (Fig. 11b), reducing the net shortwave radiation by -15.6 % (Fig. 12a) due to the
increased outgoing shortwave radiation. Changes in LAI, longwave radiation, and near-surface temperature follow similar
patterns (Figs. 11a, 12b, and 12f). In the southwest, where LAI is increased, there is a decrease in net longwave radiation and
cooler near-surface temperature. Conversely, regions with reduced LAI in the rest of Dry Chaco result in increased net
longwave radiation and warmer temperature. This can be explained by the reduced vegetation cover, which diminishes
295 shading and leads to surface warming and increased outgoing longwave radiation. The opposite effect occurs in areas with
higher LAI. Although area-averaged values at local level tend to be small due to compensating positive and negative
changes, temperature changes can reach values of up to ±0.6 °C. It is worth noting that the overall reduction in net total
radiation is also evident in the generally weaker turbulent surface fluxes (Fig. 12d-e). Latent heat decays by -4.2 %, while
sensible heat decreases by -11 % on average.

300

The agricultural expansion imposed in Dry Chaco has weak remote effects on the energy budget of Humid Chaco (Fig. 12).
The net radiation presents a slight increase consistent with the overall rise in the net shortwave radiation (Fig. 12a-c). The
spatial pattern of changes in latent heat and sensible heat are similar but of opposite signs, with latent heat decreasing by -1.1
% and sensible heat increasing by 2.7 % (Figs. 12d-e). The near-surface temperature shows a slight warming that can be with
305 increased sensible heat (Fig. 12f).

3.2.2 Effects on the water cycle

The extensive expansion of crops and grasslands in Dry Chaco results in generally drier summers in the Gran Chaco (Fig.
13). The areas that experienced direct LULCCs (local effects) present a decay in summer precipitation of -7 % on average,
and -9.3 % in soil moisture. The overall drier soils cause a reduction in evapotranspiration of -4.2 % with a spatial
310 distribution of changes similar to those observed for precipitation and soil moisture, except in the southeast of the Dry
Chaco. Similarly, runoff is reduced by -5 % on average. While the average reductions in water balance components represent
less than 10 % in magnitude, nearly half of the area with LULCCs exhibit significant negative changes of approximately -30
%. These substantial changes have the potential for a significant impact on the region, considering its arid nature.

The overall remote effects in the Humid Chaco region result in drier summers, similar to those observed in Dry Chaco but with lesser intensity (Fig. 13). The changes in precipitation indicate a general tendency towards increased dryness in most parts of the Humid Chaco, except for isolated areas experiencing significant increases (Fig. 13a). On average, summer precipitation decreases by -4 %, although there are areas with changes of up to ±30 mm month^{-1}. These changes in precipitation are accompanied by corresponding patterns in soil moisture, which also show a slight average decrease of about -1.2 % (Fig. 13b). Furthermore, evapotranspiration experiences an average reduction of -1.1 %, with localised decreases of up to -8 % in specific parts of the Humid Chaco. The overall drier conditions contribute to a reduction in runoff by about -6.2 % on average. Interestingly, this reduction is greater in the Humid Chaco than the Dry Chaco (-4.5 %). In summary, our results suggest that the expansion of agriculture in Dry Chaco intensifies the aridity of this already dry region and extends drier conditions into the Humid Chaco.

3.3 Process-based analysis

The results of the experiments consistently demonstrate that agricultural expansion in the Dry Chaco region leads to drier and warmer summers, regardless of the magnitude of the agricultural expansion. Figure 14 presents a schematic diagram summarising our interpretation of the key processes involved.

The intensification of agriculture in the Dry Chaco region brings about significant variations in biophysical properties, particularly LAI and albedo. While stomatal resistance is also greatly reduced, which would facilitate plant transpiration, its impact remains limited due to the water-limited regime. Consequently, the main focus lies on the effect of reduced LAI, leading to increased surface temperature due to decreased vegetation radiation sheltering. This rise in temperature increases the outgoing longwave radiation, resulting in a decrease in net longwave radiation. Conversely, the increased albedo decreases the net shortwave radiation by reflecting a greater portion of incoming shortwave radiation. These changes in the energy budget consequently lead to a reduction in net surface radiation, aligning with the feedback mechanisms proposed by Eltahir (1998), Seneviratne et al. (2010), and Santanello et al. (2018).

The changes in net surface radiation are counterbalanced by the sum of latent and sensible fluxes, with soil heat flux considered negligible over longer time periods. Thus, the decrease in net radiation is equivalent to a decrease in the combined latent and sensible heat fluxes. This total energy flux from the land surface into the atmosphere represents the moist static energy (MSE), characterising the overall energy within the atmospheric boundary layer. Consequently, a reduction in net radiation, and therefore, a decline in available energy at the land surface, can be associated with less energetic conditions in the boundary layer. This, in turn, influences the dynamics of the planetary boundary layer and diminishes the generation of convective precipitation (Eltahir and Pal, 1996; Eltahir, 1998). Moreover, as suggested by Williams and Renno (1993), an increase in the planet boundary layer MSE should result in higher Convective Available Potential Energy (CAPE) directly linked to storm development. In our simulations, we observe the opposite scenario:

reduced MSE implies lower CAPE, which can lead to reduced convective rainfall. This decrease in precipitation subsequently contributes to a decline in soil moisture. This creates a feedback loop since dry soil absorbs significantly less solar radiation than moist soil.

4 Discussion and conclusions

The Gran Chaco region has two dominant ecoregions: Dry Chaco and Humid Chaco. The first one, particularly in the last decades, has been experiencing an intensive deforestation process due to agricultural expansion with important environmental consequences. This study explores the dominant LULCCs in Dry Chaco from 2001 to 2015 and their effect on the regional climate. Furthermore, we examine other effects that may develop if the intensive agricultural expansion (of crop and grassland) within Dry Chaco continues. To this end, using different land cover maps, three sets of simulations (ensembles) were conducted using the WRF model from January 2014 to June 2016. The first ensemble employed the MODIS land cover map corresponding to 2015 (CONTROL). The second one used the MODIS land cover map corresponding to 2001 (PAST). The third one employed a modified version of the 2015 land cover map where the existing crop and pasture areas in 2015 within Dry Chaco were expanded (FUTURE).

The performance of the CONTROL simulation was assessed by comparing simulated precipitation, near-surface and root zone soil moisture, and 2-m temperature with gridded observations or satellite estimates. The evaluation demonstrates good skills of the WRF Model for the region of interest. Simulated precipitation shows good resemblance with observations in Gran Chaco, with minor negative biases in the Humid Chaco. Near-surface and root-zone soil moisture closely matches the products derived from remotely sensed data in the Gran Chaco, although, consistent with negative precipitation biases, drier biases are observed in the Humid Chaco. The correlation coefficients for near-surface temperature indicate a strong agreement with observations in the Gran Chaco, although with somewhat larger seasonal variability.

The MODIS maps reveal that the dominant land cover categories in the Dry Chaco include savanna, woody savanna, forest, grassland, shrubland, and cropland. Over the period from 2001 to 2015, land cover changes were observed in 18% of the entire Chaco region. These changes can be categorised as deforestation (52 %), illogical (17 %), and other (31 %). Agricultural lands, specifically cropland and grassland, experienced a sustained increase in the region particularly until 2007. Land cover changes due to deforestation processes are found in the central-east, northeast, and western boundaries of the Dry Chaco. The changes were observed in small fragmented areas, with deforestation primarily associated with decreases in leaf area index (LAI), increases in albedo, and reduced stomatal resistance. These findings align with other studies (e.g., Jiang et al. 2021), which reported that deforestation leads to lower LAI and higher surface albedo. In other areas where different land cover changes occurred (from open shrubland to barren, from grassland to cropland, among others), some biophysical properties show opposite trends, resulting in a heterogeneous pattern of property changes.

380

The simulations show that the heterogeneous LULCCs from 2001 to 2015 and the associated changes in biophysical properties led to uneven distribution of positive and negative changes in radiation fluxes, particularly affecting net radiation, sensible heat flux, and latent heat flux. While there were average reductions in net radiation and sensible heat at the local level, latent heat changes were minor. Spatially, changes in sensible heat influenced near-surface temperature, leading to
385 warming in deforested areas and cooling in areas with other LULCCs (green grid cells in Fig. 2c). The changes in biophysical properties and in the energy budget also affected the water cycle, resulting in overall drier conditions in the Dry Chaco. Precipitation exhibited significant changes, with both decreases and increases observed in different areas. Soil moisture followed the pattern of precipitation, displaying net local negative changes. The changes in precipitation and soil moisture are reflected in the evapotranspiration and the total runoff, all experiencing net negative changes. The findings
390 suggest that the observed land cover changes weakened the water cycle in the Dry Chaco, contributing to drier summers and increased vulnerability to extreme events in this arid region.

At present, there is no indication that deforestation will slow down. The possible consequences for the regional climate are explored with a new set of simulations using a land cover map that assumes an agricultural expansion of the existing crop
395 and pasture areas over savannas, woody savannas, forests, and shrublands, within Dry Chaco. Consistent with the effects observed for the LULCCs associated with deforestation in the OBS_LULCC scenario, a general decrease in LAI and stomatal resistance and an increase in albedo was observed at the local level.

The expansion of agriculture in the Dry Chaco region resulted in significant changes in the energy budget, with further
400 reductions in net radiation and weakening of the turbulent surface fluxes. These changes had local effects on the water cycle, causing drier conditions with decreased precipitation, soil moisture, evapotranspiration, and runoff. The extensive expansion of crops and grasslands in the Dry Chaco led to generally drier summers in the simulations, particularly in areas that experienced land use and land cover changes. These changes had substantial negative impacts on the water balance components, with significant reductions in precipitation, soil moisture, evapotranspiration, and runoff. The aridity of the
405 already dry Dry Chaco region was further intensified, with potential implications for its ecosystems and water resources. Furthermore, the expansion of agriculture had remote effects on the Humid Chaco, extending the drier conditions into this region. The Humid Chaco also experienced reduced precipitation, soil moisture, evapotranspiration, and runoff, although to a lesser extent than the Dry Chaco. These findings highlight the complex interactions between land use, land cover changes, and the energy and water cycles, emphasising the need for sustainable land management practices in the Chaco region to
410 mitigate the impacts of agricultural expansion and preserve these ecosystems' ecological and hydrological integrity.

Lastly, our results indicate that the expansion of agriculture and corresponding deforestation processes alter the regional hydroclimate through local, non-local, and remote changes of different magnitudes, leading to austral summers with lower

precipitation and drier and warmer soils. Although our simulations are subject to uncertainties, the results suggest that the

415   current land-use practices over Dry Chaco may not be sustainable in the long-term.

Data availability

The observational datasets used in this study are freely available online. The MODIS MCD12C1 product is available at https:/lpdaac.usgs.gov/products/mcd12c1v006/. The CPC dataset is available at https://psl.noaa.gov/data/gridded/data.cpc.globalprecip.html. The CRU TS v. 4.03 dataset is available at

420   https://dx.doi.org/10.5285/10d3e3640f004c578403419aac167d82. WFDEI dataset is available at https://rda.ucar.edu/datasets/ds314.2/dataaccess, SMOPS dataset is available at https://www.ospo.noaa.gov/Products/land/smops, H14-SM-DAS-2 dataset can be required at https://hsaf.meteoam.it/User/UserSupport. Simulations are available upon request.

Author contribution

425   MAB, OVM, and EHB designed the study. MAB performed the simulations, computed the results, and prepared the original manuscript. All authors analysed and discussed the results and contributed to the subsequent versions of the paper. OVM, MAL, and EHB acquired funding and resources.

Competing interests

The authors declare that they have no conflict of interest.

430   **Acknowledgements**

We thank Prof. José Paruelo for his comments on the MODIS classification of land covers. This research was supported by the projects CAI+D-2016-50020150100005LI from the UNL. OVM and MAL acknowledge further support from the grants PICT-2019-2019-03982 and PICT-2019-2019-00481 from the ANPCYT, PIP 11220200102257CO from the CONICET, and PEICID-2021-028 from the ASaCTeI. EHB was supported by NOAA grant NA19NES4320002 (Cooperative Institute for

435   Satellite Earth System Studies -CISESS) at the University of Maryland/ESSIC. He also thanks the Fulbright Commission for facilitating the last stages of this research.

References

Albergel, C., De Rosnay, P., Gruhier, C., Muñoz-Sabater, J., Hasenauer, S., Isaksen, L., Kerr Y. and Wagner, W.: Evaluation of remotely sensed and modelled soil moisture products using global ground-based in situ observations, Remote Sens.
440 Environ., 118, 215-226, https://doi.org/10.1016/j.rse.2011.11.017, 2012.

Baldi, G., Houspanossian, J., Murray, F., Rosales, A., Rueda, C., and Jobbágy, E.: Cultivating the dry forests of South America: Diversity of land users and imprints on ecosystem functioning, J. Arid Environ.., 123, 47-59, https://doi.org/10.1016/j.jaridenv.2014.05.027, 2015.

Boletta, P. E., Ravelo, A. C., Planchuelo, A. M., and Grilli, M.: Assessing deforestation in the Argentine Chaco, Forest Ecol.
445 Manag., 228(1-3), 108-114, https://doi.org/10.1016/j.foreco.2006.02.045, 2006.

Bucher, E.H.: Chaco and Caatinga — South American Arid Savannas, Woodlands and Thickets, In: Ecology of Tropical Savannas, Ecological Studies, vol 42, edited by: Huntley, B.J., Walker, B.H., Springer, Berlin, Heidelberg, Germany, 191-211, https://doi.org/10.1007/978-3-642-68786-0_4., 1982.

Bucher, E. H., and Huszar, P. C.: Sustainable management of the Gran Chaco of South America: ecological promise and
450 economic constraints, J. Environ. Manage., 57(2), 99-108, https://doi.org/10.1006/jema.1999.0290, 1999.

Cai, S., Liu, D., Sulla-Menashe, D., and Friedl, M. A.: Enhancing MODIS land cover product with a spatial–temporal modeling algorithm, Remote Sens. Environ., 147, 243-255, https://doi.org/10.1016/j.rse.2014.03.012, 2014.

Chen, F., and Dudhia J.: Coupling an advanced land surface hydrology model with the Penn State–NCAR MM5 modeling system. Part I: Model implementation and sensitivity, Mon. Weather. Rev., 129, 569–585, https://doi.org/10.1175/1520-
455 0493(2001)129<0569:CAALSH>2.0.CO;2, 2001.

Chen, F., Mitchell, K., Schaake, J., Xue, Y., Pan, H. L., Koren, V., Duan, Q. Y., Ek, M. and Betts, A.: Modeling of land surface evaporation by four schemes and comparison with FIFE observations. J. Geophys. Res-Atmos., 101(D3), 7251-7268, https://doi.org/10.1029/95JD02165,1996.

Dirmeyer, P.: Using a global soil wetness dataset to improve seasonal climate simulation, J. Climate, 13, 2900-2922,
460 https://doi.org/10.1175/1520-0442(2000)013<2900:UAGSWD>2.0.CO;2, 2000.

Dros, J. M.: Managing the Soy Boom: Two scenarios of soy production, Amsterdam, AID Environment, 63 pp., 2004.

Eltahir, E. A. B., and Pal, J. S.: Relationship between surface conditions and subsequent rainfall in convective storms, J. Geophys. Res., 101(D21), 26237– 26245, https://despecially thankD01380, 1996.

Eltahir, E. A. B.: A Soil Moisture–Rainfall Feedback Mechanism: 1. Theory and observations, Water Resour. Res., 34(4),
465 765– 776, https://doi.org/10.1029/97WR03499, 1998.

Fehlenberg, V., Baumann, M., Gasparri, N. I., Piquer-Rodriguez, M., Gavier-Pizarro, G., and Kuemmerle, T.: The role of soybean production as an underlying driver of deforestation in the South American Chaco, Global Environ. Chang., 45, 24-34, https://doi.org/10.1016/j.gloenvcha.2017.05.001, 2017.

Gasparri, N. I., and Grau, H. R.: Deforestation and fragmentation of Chaco dry forest in NW Argentina (1972−2007), Forest
470 Ecol. Manag., 258(6), 913-921, https://doi.org/10.1016/j.foreco.2009.02.024, 2009.

Hansen, M. C., Potapov, P. V., Moore, R., Hancher, M., Turubanova, S. A., Tyukavina, A., Thaus, D., Stehman, S. V.,
Goetz, S. J., Loveland, T. R., Kommareddy, A., Egorov, A., Chini, L., Justice, C. O. and Townshend, J.: High-resolution
global maps of 21st-century forest cover change, Science, 342(6160), 850-853, doi: 10.1126/science.1244693, 2013.

Gónzalez, R. and Woods, R.: Digital Image Processing. Addison-Wesley Longman Publishing Co, Boston, United States,
475 503 pp., ISBN:978-0-201-11026-5, 1993.

Harris, I., Osborn, T.J., Jones, P. and Lister, D.: Version 4 of the CRU TS monthly high-resolution gridded multivariate
climate dataset, Scientific Data, 7(109), 1−18, https://doi.org/10.1038/s41597-020-0453-3, 2020.

Hoffman, R. N., and Kalnay, E.: Lagged average forecasting, an alternative to Monte Carlo forecasting, Tellus A, 35(2),
100-118, https://doi.org/10.3402/tellusa.v35i2.11425, 1983.

480 Jiang, Y., Wang, G., Liu, W., Erfanian, A., Peng, Q., and Fu, R.: Modeled response of South American climate to three
decades of deforestation, J. of Climate, 34(6), 2189-2203, https://doi.org/10.1175/JCLI-D-20-0380.1, 2021.

Jobbágy, E., Nosetto, M ., Santoni, C. and Baldi, G.: El desafío ecohidrológico de las transiciones entre sistemas leñosos y
herbáceos en la llanura Chaco-Pampeana, Ecología austral, 18(3), 305-322, avialable at
https://ojs.ecologiaaustral.com.ar/index.php/Ecologia_Austral/article/view/1377 (last access: 19 May 2023), 2008.

485 Kuemmerle, T., Altrichter, M., Baldi, G., Cabido, M., Camino, M., Cuellar, E., Cuellar, R. L., Decarre, J., Díaz, S., Gasparri,
I., Gavier-Pizarro, G., Ginzburg, R., Giordano, A. J., Grau, H. R., Jobbagy, E., Leynaud, G., Macchi, L., Mastrangelo, M.,
Matteucci, S. D., Noss, A., Paruelo, J., Piquer-Rodriguez, M., Romero-Muñoz, A., Semper-Pascual, A., Thompson, J.,
Torrella, S., Torres, R., Volante, J. N., Yanosky, A.and Zak, M.: Forest conservation: remember gran chaco, Science,
355(6324), 465-465, doi: 10.1126/science.aal3020, 2017.

490 Lee, S. J., and Berbery, E. H.: Land cover change effects on the climate of the La Plata Basin, J. Hydrometeorol., 13 (1), 84-
102, https://doi.org/10.1175/JHM-D-11-021.1, 2012.

Liang L, and Gong, P.: An assessment of MODIS Collection 5 global land cover product for biological conservation studies.
In: 2010 18th international conference on geoinformatics, Beijing, China, 18−20 June 2010, pp 1−6,
https://doi.org/10.1109/GEOINFORMATICS.2010.5567991, 2010.

495 Liu, J., Zhan, X., Hain, C., Yin, J., Fang, L., Li, Z., and Zhao, L.: NOAA soil moisture operational product system (SMOPS)
and its validations. In 2016 IEEE International Geoscience and Remote Sensing Symposium (IGARSS) (pp. 3477-3480).
IEEE, https://doi.org/10.1109/IGARSS.2016.7729899, 2016.

Mahmood, R., Pielke Sr, R. A., Hubbard, K. G., Niyogi, D., Bonan, G., Lawrence, P., McNider, R., McAlpine, C., Etter, A.,
Gameda, S., Qian, B., Carleton, A., Beltran-Przekurat, A., Chase, T., Quintanar, A., Adegoke, J., Vezhapparambu, S.,
500 Conner, G., Asefi, S, Sertel, E., Legates, D., Wu, Y., Hale, R., Frauenfeld, O., Watts, A., Shepherd, M., Mitra, C.,
Anantharaj, V., Fall, S., Lund, R., Treviño, A., Blanken, P., Du, J., Chang, H-I, Leeper, R., Nair, U., Dobler, S., Deo, R.,

and Syktus, J.: Impacts of land use/land cover change on climate and future research priorities, Bull. Am. Meteorol. Soc., 91(1), 37-46, https://doi.org/10.1175/2009BAMS2769.1, 2010.

Mahmood, R., Pielke, R.A., Sr., Hubbard, K.G., Niyogi, D., Dirmeyer, P.A., McAlpine, C., Carleton, A.M., Hale, R.,
505   Gameda, S., Beltrán-Przekurat, A., Baker, B., McNider, R., Legates, D.R., Shepherd, M., Du, J., Blanken, P.D., Frauenfeld, O.W., Nair, U.S. and Fall, S..: Land cover changes and their biogeophysical effects on climate, Int. J Climatol., 34(4), 929-953, doi:10.1002/joc.3736, 2014.

Martinez, J., Dominguez, F. and Miguez-Macho, G.: Impacts of a Groundwater Scheme on Hydroclimatological Conditions over Southern South America, J. Hydrometeorol., 17(11), 2959-2978, doi:10.1175/JHM-D-16-0052.1, 2016.

510   Miguez-Macho, G., Fan, Y., Weaver, C., Walko, R. and Robock, A.: Incorporating water table dynamics in climate modeling: 1. Water table observations and equilibrium water table simulations, J. Geophys. Res., 112, D10125, https://doi.org/10.1029/2006JD008111, 2007.

Müller, O. V., Berbery, E. H., Alcaraz Segura, D., and Ek, M. B.: Regional model simulations of the 2008 drought in southern South America using a consistent set of land surface properties, J. Clim.,   27(17), 6754-6778,
515   https://doi.org/10.1175/JCLI-D-13-00463.1, 2014.

Müller, O. V., Lovino, M. A., and Berbery, E. H.: Evaluation of WRF model forecasts and their use for hydroclimate monitoring over southern South America, Weather Forecast., 31(3), 1001-1017., https://doi.org/10.1175/WAF-D-15-0130.1, 2016.

Müller, O. V., Vidale, P. L., Vannière, B., Schiemann, R., Senan, R., Haarsma, R. J., and Jungclaus, J. H.: Land–Atmosphere
520   Coupling Sensitivity to GCMs Resolution: A Multimodel Assessment of Local and Remote Processes in the Sahel Hot Spot, J. Clim., 34(3), 967-985, doi:10.1175/JCLI-D-20-0303.1, 2021a.

Müller, O., Vidale, P. L., Vannière, B., Schiemann, R., and McGuire, P.: Does the HadGEM3-GC3.1 GCM overestimate land precipitation at high resolution? A constraint based on observed river discharge. J. Hydrometeorol., 22, 8, 2131-2151. https://doi.org/10.1175/JHM-D-20-0290.1, 2021b.

525   Nori, J., Torres, R., Lescano, J. N., Cordier, J. M., Periago, M. E., and Baldo, D.: Protected areas and spatial conservation priorities for endemic vertebrates of the Gran Chaco, one of the most threatened ecoregions of the world, Divers. Distrib., 22(12), 1212-1219, https://doi.org/10.1111/ddi.12497, 2016.

Paruelo, J. M., Guerschman, J. P., and Verón, S. R.: Agricultural expansion and changes in land use, Ciencia Hoy, 15, 14–23, 2005 (in Spanish).

530   Piquer-Rodríguez, M., Torella, S., Gavier-Pizarro, G., Volante, J, Somma, D., Ginzburg, R., and Kuemmerle, T.: Effects of past and future land conversions on forest connectivity in the Argentine Chaco. Landscape Ecol., 30, 817–833, https://doi.org/10.1007/s10980-014-0147-3, 2015.

Portillo-Quintero, C. A., and Sánchez-Azofeifa, G. A.: Extent and conservation of tropical dry forests in the Americas, Biol. Conserv., 143(1), 144-155, https://doi.org/10.1016/j.biocon.2009.09.020, 2010.

535 Ruscica, R., Menéndez, C. and Sörensson, A.: Land surface-atmosphere interaction in future South American climate using a multi-model ensemble, Atmos. Sci. Lett., 17: 141-147, https//doi.org/10.1002/asl.635, 2016.

Saha, S., Moorthi, S., Wu, X., Wang, J., Nadiga, S., Tripp, P., Behringer, D., Hou, Y., Chuang, H., Iredell, M., Ek, M., Meng, J., Yang, R., Mendez, M. P., van den Dool, H., Zhang, Q., Wang, W., Chen, M., and Becker, E.: The NCEP Climate Forecast System Version 2, J. Clim., 27(6), 2185-2208, https://doi.org/10.1175/JCLI-D-12-00823.1, 2014.

540 Salazar, A., Baldi, G., Hirota, M., Syktus, J., and McAlpine, C.: Land use and land cover change impacts on the regional climate of non-Amazonian South America: A review, Glob. Planet. Change., 128, 103-119, https://doi.org/10.1016/j.gloplacha.2015.02.009, 2015.

Santanello, J. A., Dirmeyer, P. A., Ferguson, C. R., Findell, K. L., Tawfik, A. B., Berg, A., Ek, M., Gentine, P., Guillod, B. P., van Heerwaarden, C., Roundy, J., and Wulfmeyer, V.: Land–atmosphere interactions: The loco perspective. Bull. Am.
545 Meteorol. Soc., 99(6), 1253–1272. https://doi.org/10.1175/bams-d-17-0001.1, 2018.

Seneviratne, S. I., Corti, T., Davin, E. L., Hirschi, M., Jaeger, E. B., Lehner, I., Orlowsky, B., and Teuling, A. J.: Investigating soil moisture–climate interactions in a changing climate: A Review. Earth Sci. Rev., 99(3–4), 125–161, https://doi.org/10.1016/j.earscirev.2010.02.004, 2010.

Sirimarco, X., Barral, M. P., Villarino, S. H., and Laterra, P.: Water regulation by grasslands: A global meta-analysis,
550 Ecohydrology, e19-34, https://doi.org/10.1002/eco.1934, 2018.

Spennemann, P. and Saulo, A.: An estimation of the land-atmosphere coupling strength in South America using the Global Land Data Assimilation System, Int. J. Climatol., 35, 4151-4166, https://doi.org/10.1002/joc.4274, 2015.

University of East Anglia Climatic Research Unit; Harris, I.C.; Jones, P.D. (2020): CRU TS4.03: Climatic Research Unit (CRU) Time-Series (TS) version 4.03 of high-resolution gridded data of month-by-month variation in climate (Jan. 1901-
555 Dec. 2018). Centre for Environmental Data Analysis, 22 January 2020. https://dx.doi.org/10.5285/10d3e3640f004c578403419aac167d82, 2020.

Volante, J. N., Mosciaro, M. J., Gavier-Pizarro, G. I., and Paruelo, J. M.. Agricultural expansion in the Semiarid Chaco: Poorly selective contagious advance, Land use policy, 55, 154-165, https://doi.org/10.1016/j.landusepol.2016.03.025, 2016.

Weedon, G. P., Balsamo, G., Bellouin, N., Gomes, S., Best, M. J., and Viterbo, P.: The WFDEI Meteorological Forcing
560 Data. Research Data Archive at the National Center for Atmospheric Research, Computational and Information Systems Laboratory, doi: 10.5065/486N-8109, 2018.

Williams, E., and Renno, N.: An Analysis of the Conditional Instability of the Tropical Atmosphere. Mon. Wea. Rev., 121, 21–36, https://doi.org/10.1175/1520-0493(1993)121<0021:AAOTCI>2.0.CO;2, 1993.

Zak, M. R., Cabido, M., Cáceres, D., and Díaz, S.: What drives accelerated land cover change in central Argentina?
565 Synergistic consequences of climatic, socioeconomic, and technological factors. Enviro. Manage., 42(2), 181-189, https://doi.org/10.1007/s00267-008-9101-y, 2008.

Parameter	Description
Region	Southeastern South América
Grid resolution	12 km
Grid size	320 x 283 grid points
N° of vertical levels	38
Period	January 2014 – June 2016
Integration time step	60 s
Dynamic solver	ARW
Boundary conditions	CFSv2 (Saha et al. 2011)
Microphysics	Eta (Ferrier) (Rogers y otros, 2001)
Cumulus convection	Betts-Miller-Janjic scheme(Janjic, 1994, 2000)
Surface layer	MM5 Monin-Obukhov scheme (Jiménez et al, 2012)
Land surface model	Noah-MP (Niu y otros, 2011)
Planet boundary layer	No boundary-layer
Shortwave radiation	Dudhia scheme (Dudhia, 1989)
Longwave radiation	Rapid Radiative Transfer Model (Mlawer y otros, 1997)

Table 1. Summary of WRF configuration.

Parametrization	Selected Option
Land cover classification	MODIS - IGBP 21 Categorías
Stomatal resistance	Ball–Berry (Ball et al. 1987)
Surface layer drag coefficient calculation	Monin–Obukhov (Brutsaert, 1982)
Soil moisture factor for stomatal resistance	Noah type (Chen and Dudhia, 2001)
Runoff and groundwater	TOPMODEL with groundwater (Niu et al. 2007)
Supercooled liquid water	Standard freezing point depression (Niu and Yang 2006)
Soil permeability	Linear effect, more permeable (Niu and Yang 2006)
Radiative transfer	Modified two-stream
Ground surface albedo	CLASS (Canadian Land Surface Scheme) (Verseghy, 1991)
Precipitation partitioning between snow and rain	Jordan (Jordan, 1991)
Soil temp lower boundary condition	TBOT at 8 m from input file
Snow/soil temperature time scheme	Semi implicit

Table 2. NOAH-MP selected parametrization.

575

580
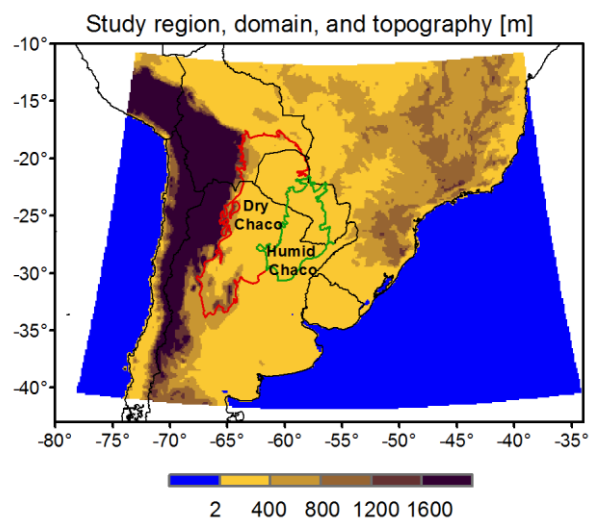
Figure 1: Model domain and topography. The coloured lines highlight the Gran Chaco subregions: Dry Chaco (red) and Humid Chaco (green).
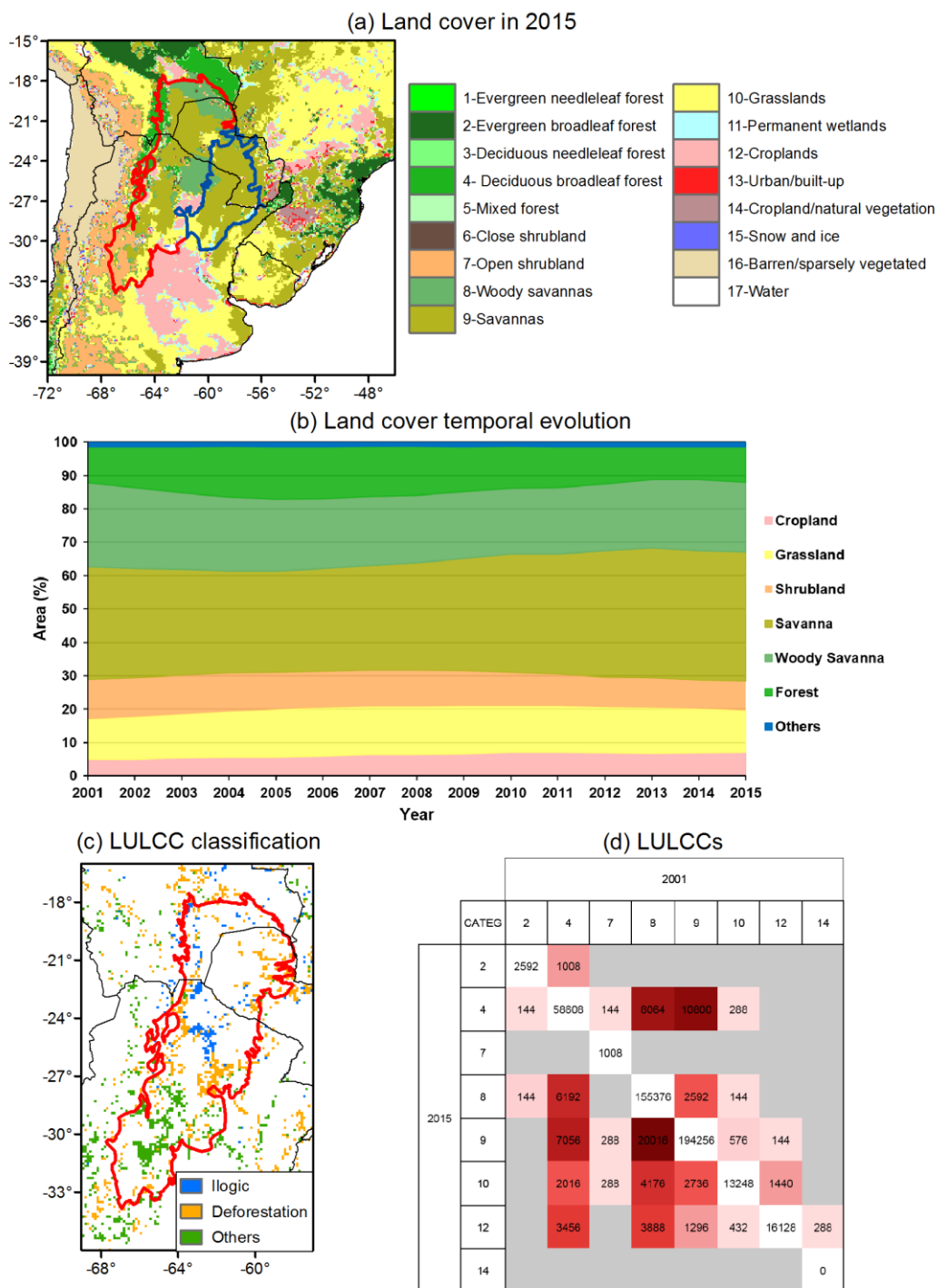
Figure 2: (a) 2015 MODIS land cover map using IGBP classification. (b) Temporal evolution of land cover in Dry Chaco. For simplicity land cover types are aggregated in fewer classes (see text). (c) LULCCs in Dry Chaco. (d) Quantification (in km²) of LULCCs in Dry Chaco from 2001 to 2015. The cell colour is proportional to its value.
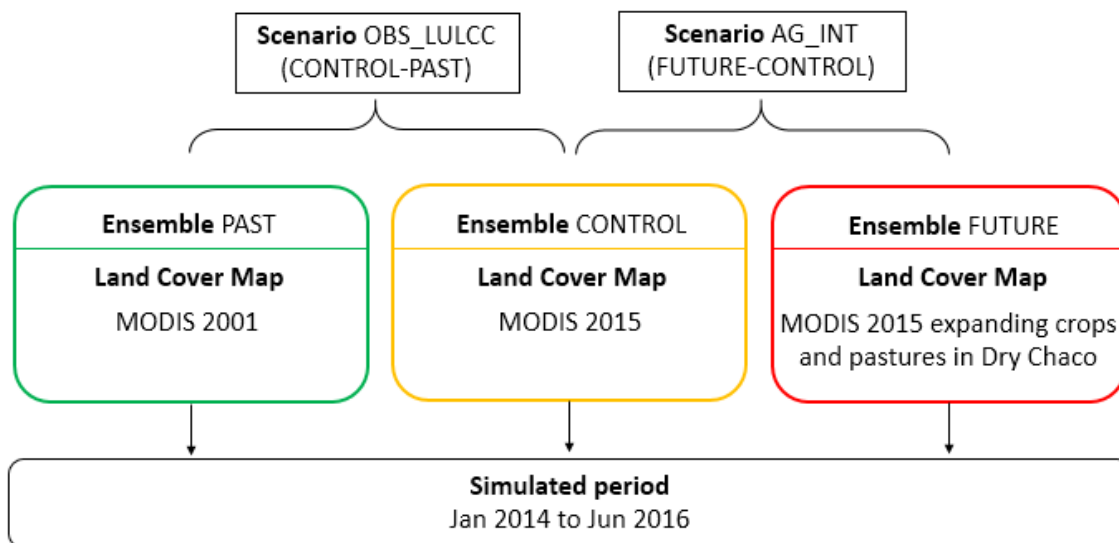
Figure 3: Experimental design.
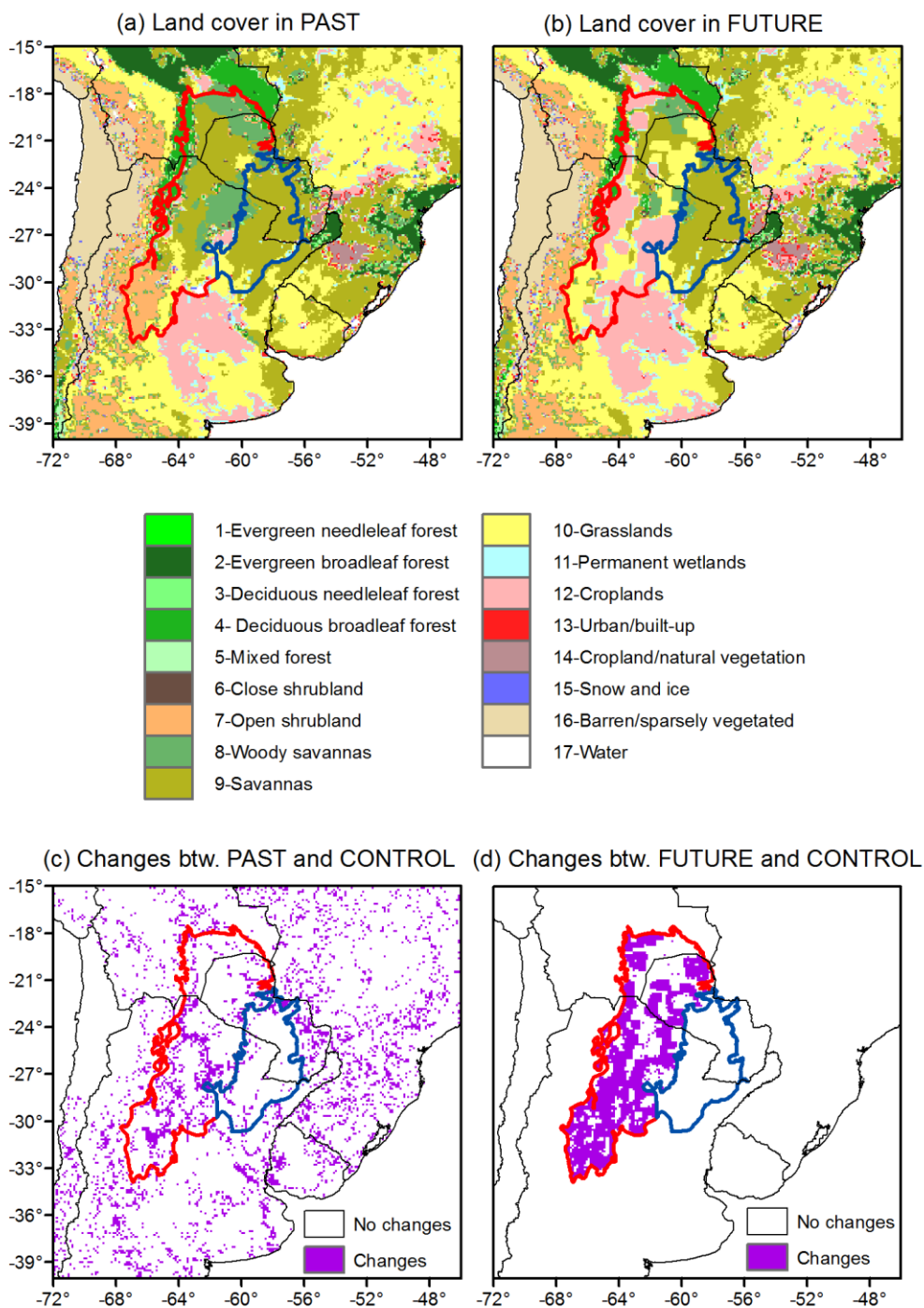
590

Figure 4: Land cover map of (a) the PAST and (b) the FUTURE ensemble, and (c-d) their respective differences with the land cover map of the CONTROL ensemble.
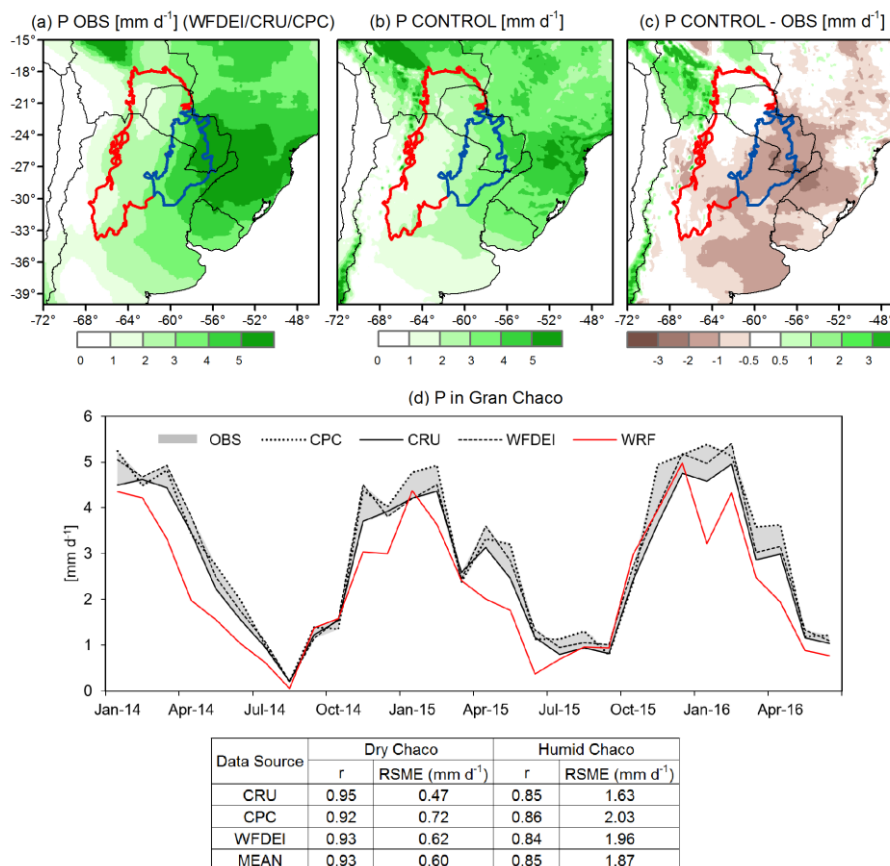
Figure 5: Time average of (a) the observed precipitation (mean between WFDEI, CRU, and CPC), (b) the CONTROL ensemble precipitation, and (c) their differences. (d) Precipitation time series averaged in the Gran Chaco region.
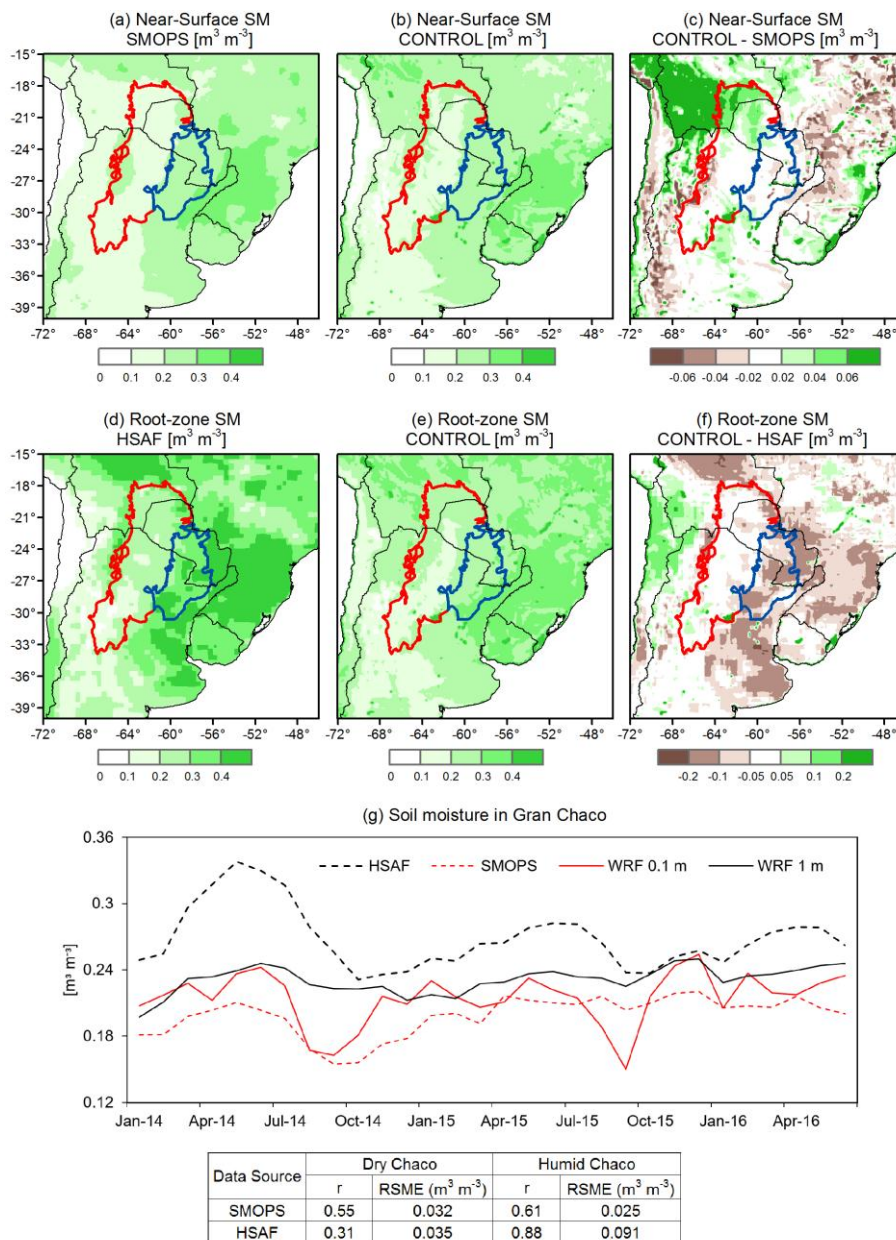
Figure 6: Time average of near-surface soil moisture for (a) the SMOPS product, (b) the CONTROL ensemble, (c) their differences, and time average of root-zone soil moisture for (d) the HSAF product, (e) the CONTROL ensemble, and (f) their differences. (g) Observed and simulated soil moisture time series averaged over the Gran Chaco.

600
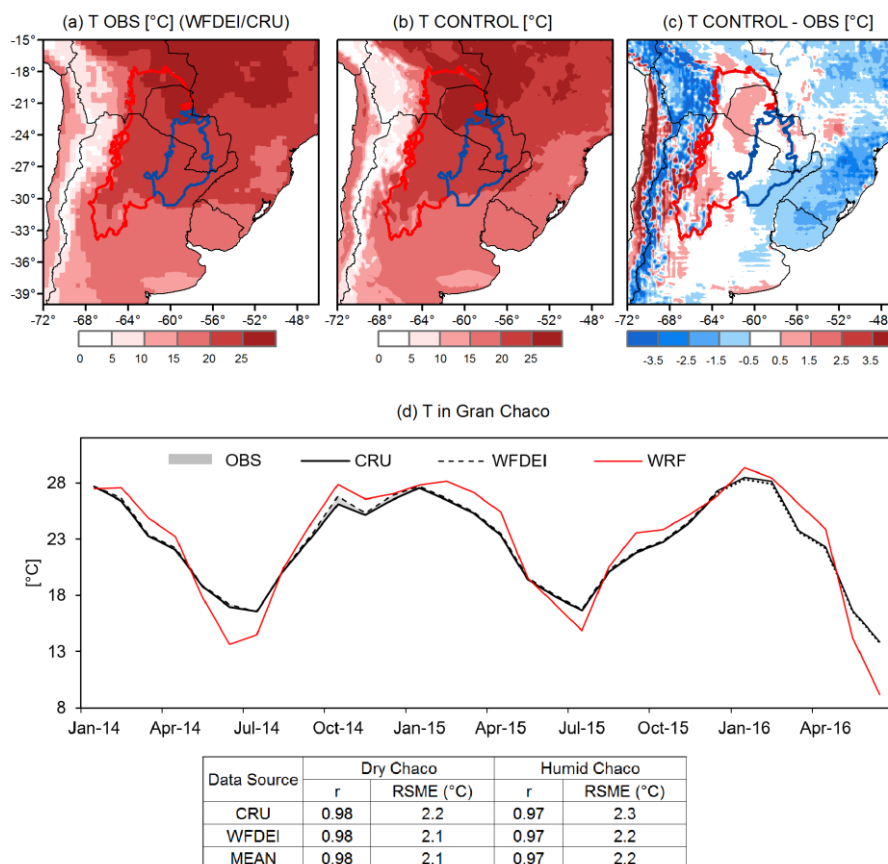
Figure 7: Time average of (a) observed 2m temperature, (b) the CONTROL ensemble 2m temperature, and (c) their differences. (d) Temperature time series averaged over the Gran Chaco.
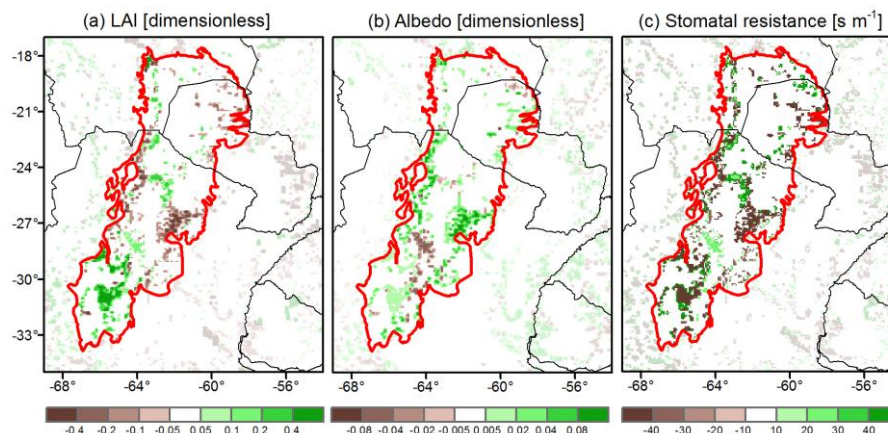
605   **Figure 8: Differences in the biophysical properties for the OBS_LULCC scenario (CONTROL-PAST): (a) LAI, (b) albedo, and (c) stomatal resistance. Opacity was used in all panels to highlight the region of interest.**
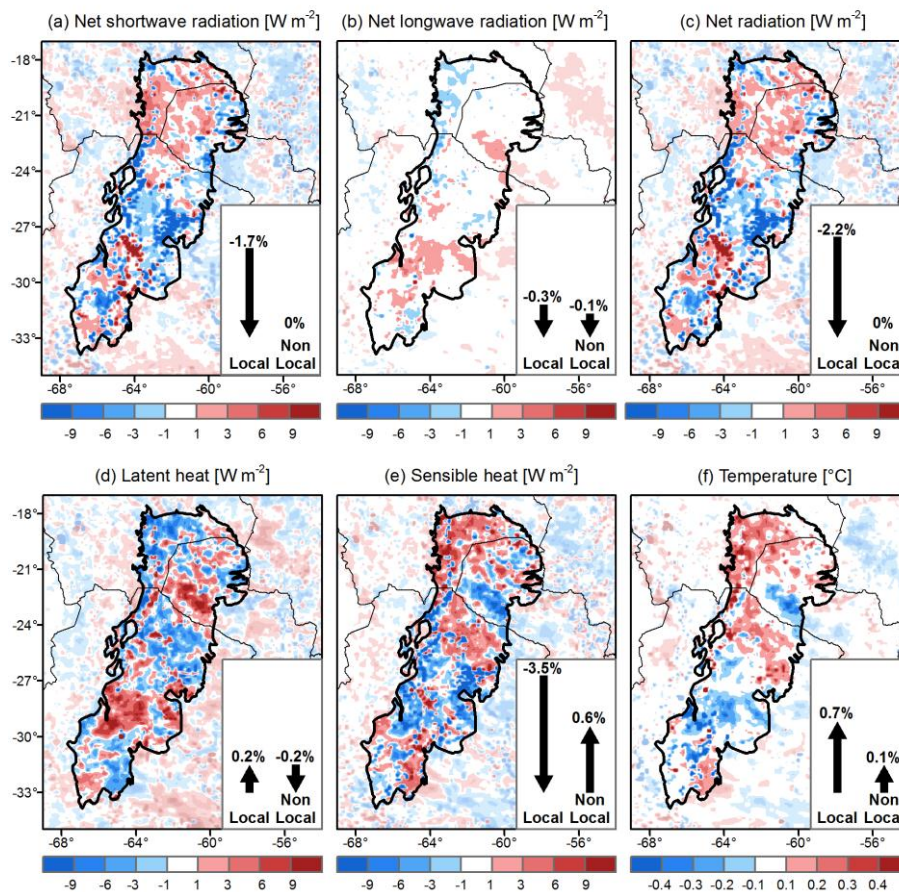
Figure 9: Differences in the summer energy budget components in the OBS_LULCC scenario (CONTROL-PAST): (a) net shortwave radiation, (b) net longwave radiation, (c) net radiation, (d) latent heat, (e) sensible heat, and (f) 2m temperature. Opacity was used to highlight the region of interest. The insets show the percentage differences averaged over grid cells with land cover changes (Local) and without land cover changes in Dry Chaco (Non-Local).

610
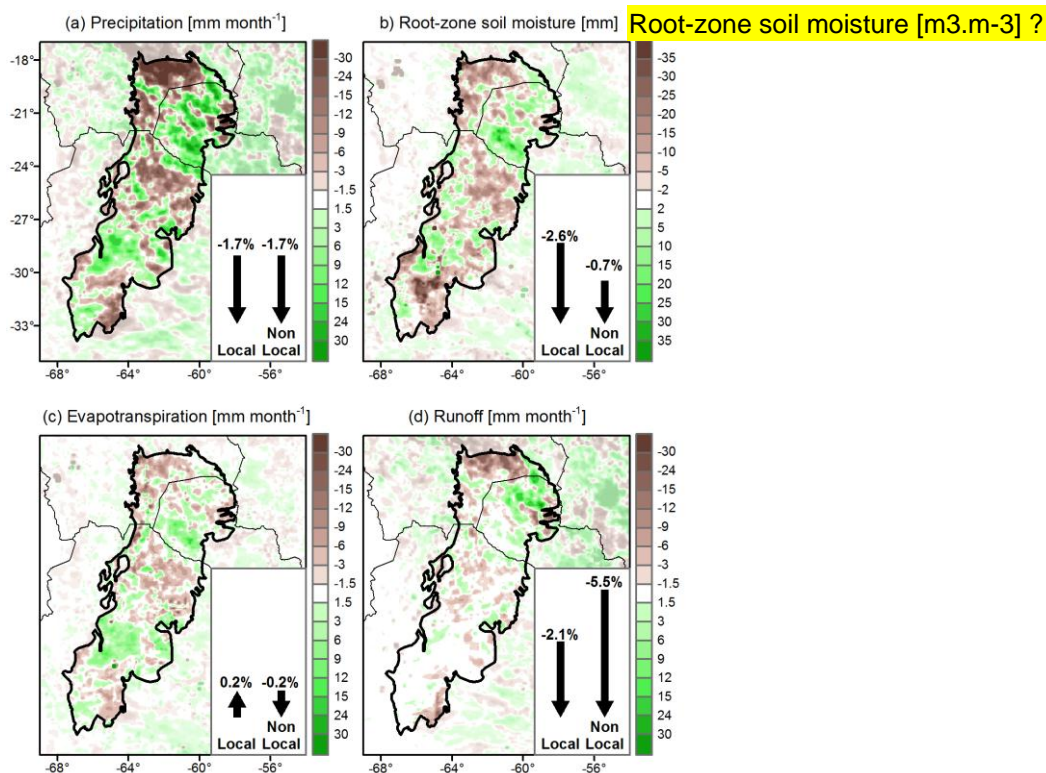
Figure 10: Differences in the summer water budget components in the OBS_LULCC scenario (CONTROL-PAST): (a) precipitation, (b) soil moisture, (c) evapotranspiration, and (d) runoff. Opacity was used to highlight the region of interest. The insets show the percentage differences averaged over grid cells with land cover changes (Local) and without land cover changes in Dry Chaco (Non-Local).

615
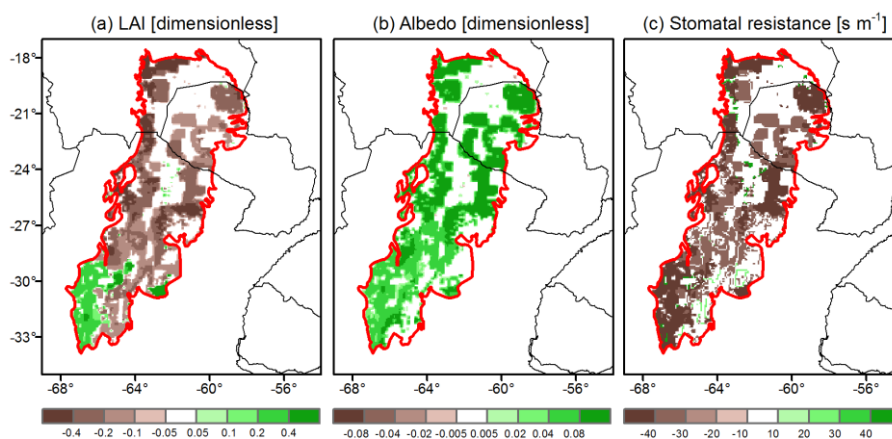
Figure 11: Differences in the biophysical properties for the AG_INT scenario (FUTURE-CONTROL): (a) LAI, (b) albedo, and (c) stomatal resistance. Opacity was used in all panels to highlight the region of interest.
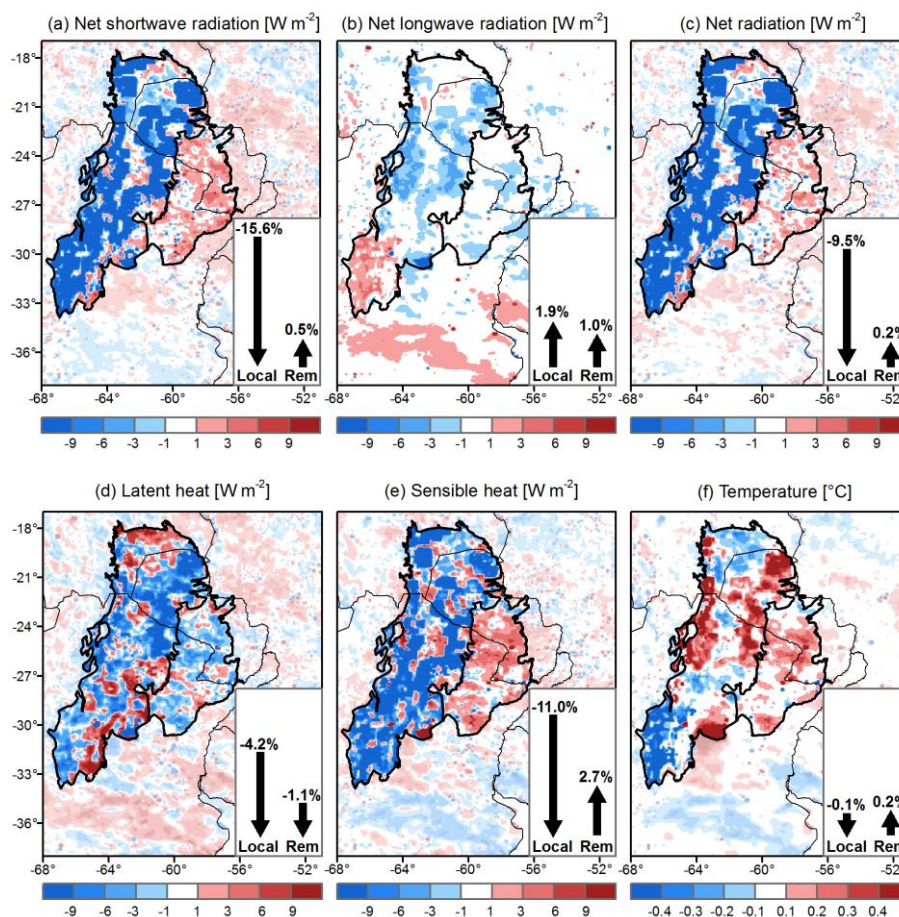
Figure 12: Differences in the summer energy budget components in the AG_INT scenario (FUTURE-CONTROL):
(a) net shortwave radiation, (b) net longwave radiation, (c) net radiation, (d) latent heat, (e) sensible heat, and (f) 2m
temperature. Opacity was used to highlight the region of interest. The insets show the percentage differences
averaged over grid cells with land cover changes in Dry Chaco (Local) and over the Humid Chaco (Rem).

620
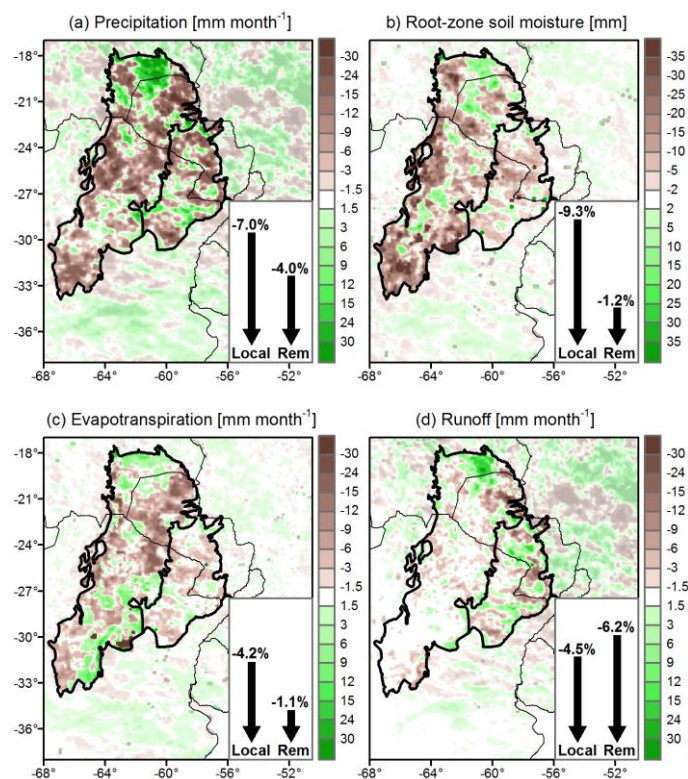
Figure 13: **Differences in the summer water budget components in the AG_INT scenario (FUTURE-CONTROL): (a) precipitation, (b) soil moisture, (c) evapotranspiration, and (d) runoff for Past experiment. Opacity was used to highlight the region of interest. The insets show the percentage differences averaged over grid cells with land cover changes in Dry Chaco (Local) and over the Humid Chaco (Rem).**

625
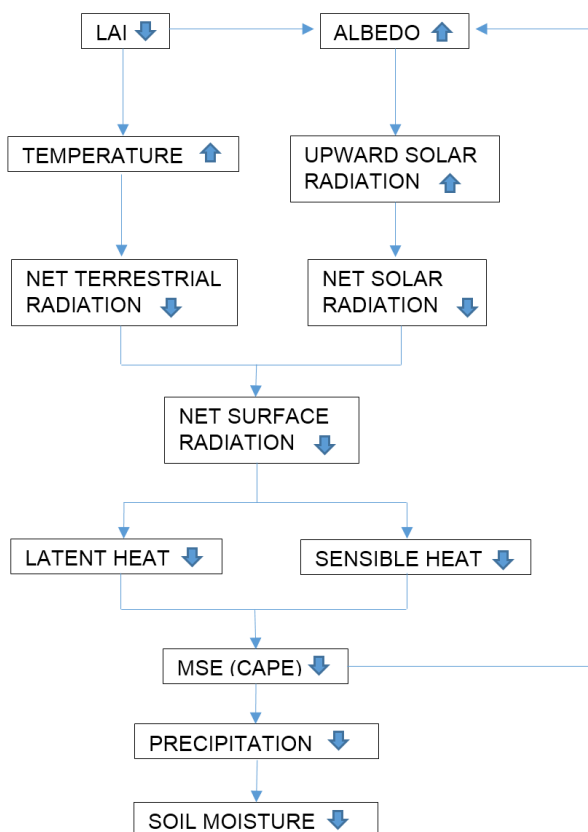
630

Figure 14: Schematic diagram of the possible land-atmosphere feedback pathway caused by agricultural expansion. Upward arrows represent increases, while downward arrows depict decreases.